Engineering Frontier Energy Levels in Donor–Acceptor Fluoren-9-ylidene Malononitriles versus Fluorenones

ARTICLE *in* THE JOURNAL OF PHYSICAL CHEMISTRY A · DECEMBER 2013

Impact Factor: 2.69 · DOI: 10.1021/jp407854r · Source: PubMed

4 AUTHORS, INCLUDING:

Paul Homnick
3M
10 PUBLICATIONS **36** CITATIONS
SEE PROFILE

Paul Lahti
University of Massachusetts Amherst
253 PUBLICATIONS **3,449** CITATIONS
SEE PROFILE

THE JOURNAL OF PHYSICAL CHEMISTRY A

Article

pubs.acs.org/JPCA

Engineering Frontier Energy Levels in Donor−Acceptor Fluoren-9-ylidene Malononitriles versus Fluorenones

Paul J. Homnick, Jonathan S. Tinkham, Raymond Devaughn, and Paul M. Lahti*

Department of Chemistry, University of Massachusetts, Amherst, Massachusetts 01003 United States

Supporting Information

ABSTRACT: Donor−acceptor molecules incorporating fluoren-9-ylidene malononitrile acceptor units conjugated to trimethoxystyrene and/or diarylamine donor units were synthesized, and their electronic spectral properties and electrochemical behaviors were evaluated by comparison to those of the analogous fluorenones. Frontier energy level and optical transition energy trends are explained based on a quantitative, modular donor−acceptor interaction model. A connectivity effect on absorption transition moment strength is also described.

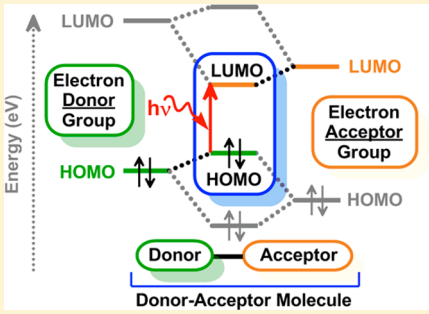

INTRODUCTION

Donor−acceptor (D−A), or "push−pull", systems have drawn much attention for potential use as electronic materials for nonlinear optical, energy harvesting, and charge transport testing.[1] Much work and molecular design strategy has aimed for specific optical transition energies (often taken as measures of band gap) as well as specific highest occupied and lowest unoccupied molecular orbital (HOMO, LUMO) energy levels in donor−acceptor compounds because of their potential utility in electronic applications.[2] Because of the high promise of molecular electronic devices, much effort continues in the design of new, synthetically simple donor−acceptor conjugated organic molecules and in the improvement of prediction of their spectral and electronic behaviors.

The inexpensive, synthetically simple and readily functionalized fluorenone (FO) has been heavily studied for its electronic spectral behavior[3] and for its role in green emission bands[4] in fluorene-based organic LEDs. There have also been a number of studies of substitution effects on fluorenone spectroscopy.[5,6] Recently, Homnick and Lahti described[7] a study in which synthetically simple 2-fluorenonyl and 2,7-fluorenonediyl acceptor units can be linked in a modular fashion to diarylamine donor groups to give consistent LUMO levels from the fluorenone unit and tunable HOMO levels from the donors. In the present report, the initial design is extended to additional fluorenone systems and especially to the stronger electron acceptor fluoren-9-ylidene malononitrile (FM). FM-based systems have lower LUMO levels relative to their FO-based analogues, decreasing all optical transition energies because the donor-controlled HOMO levels remain the same, to a first approximation. The results described below show that the use of a modular "building block" strategy produced FM-based D−A and D−A−D donor−acceptor compounds with molecular electronic properties that can be varied in a manner that is crucial for the development of new organic electronic materials.

METHODOLOGY

General Synthetic and Characterization Procedures. Fluorenone (FO) derivatives used in this study were synthesized by variations of literature routes[7,8] then converted to fluoren-9-ylidene malononitriles (FMs) by Knoevenagel condensation. All new compounds were characterized by ^{1}H NMR at 400 MHz proton (chemical shifts reported below as δ in ppm downfield of tetramethylsilane), attenuated total reflection Fourier transform infrared (ATR-FTIR) spectroscopy, and FAB high-resolution mass spectrometry; summaries are given below. Full experimental details are given in the Supporting Information. Sample purities were established by high-performance liquid chromatography (HPLC) obtained on a Buck Scientific BLC-10-11 instrument with a C18 reverse-phase column (acetonitrile, elution at 0.25 mL/min). UV−vis−NIR spectra were obtained at room temperature using a Shimadzu UV-3600 spectrophotometer.

2-(1-(3,4,5-Trimethoxyphenyl-2-ethenyl)-fluoren-9-ylidene Malononitrile (FMS). Mp 203−204 °C. ATR-IR (neat, cm^{-1}) 2220 (s, C≡N str). ^{1}H NMR (DMSO-d_6): 3.68 (s, 3 H), 3.85 (s, 6H), 6.96 (s, 2H), 7.16−7.20 (d, 1H, J = 16 Hz), 7.29−7.33 (d, 1H, J = 16 Hz), 7.43−7.47 (t, 1H, J = 16 Hz, J' = 8 Hz), 7.61−7.65 (t, 1H, J = 16 Hz, J' = 8 Hz), 7.86−7.89 (m, 3H), 8.22−8.24 (d, 1H, J = 8 Hz), 8.36 (s, 1H). ^{1}H NMR (400 MHz, $CDCl_3$): 3.89 (s, 3 H), 3.94 (s, 6H), 6.76 (s, 2H), 6.99−7.03 (d, 1H, J = 16 Hz), 7.08−7.12 (d, 1H, J = 16 Hz), 7.29−7.33 (t, 1H, J = 16 Hz, J' = 8 Hz), 7.48−7.54 (m, 3H), 7.62−7.64 (d, 1H, J = 8 Hz), 8.36−8.38 (d, 1H, J = 8 Hz), 8.50 (s,

Received: August 6, 2013
Revised: December 16, 2013
Published: December 30, 2013

   dx.doi.org/10.1021/jp407854r | J. Phys. Chem. A 2014, 118, 475−486

1H). MS (FAB): found, m/z = 420.14606; calcd for $C_{27}H_{20}N_2O_3$, m/z = 420.14684.

2,7-Bis(1-(3,4,5-trimethoxyphenyl-2-ethenyl)-fluoren-9-ylidene Malononitrile (FMDS). Mp 267−269 °C (d). ATR-IR (neat, cm^{-1}) 2225 (s, C≡N str). ^1H NMR ($CDCl_3$): 3.89 (s, 6H), 3.94 (s, 12H), 6.75 (s, 4H), 6.97−7.01 (d, 2H, J = 16 Hz), 7.07−7.11 (d, 2H, J = 16 Hz), 7.49−7.51 (d, 2H, J = 8 Hz), 7.61−7.63 (d, 2H, J = 8 Hz), 8.48 (s, 2H). MS (FAB): found m/z = 612.2260; calcd for $C_{38}H_{32}N_2O_6$, m/z = 612.22549.

2-(N,N-Diphenylamino)-fluoren-9-ylidene Malononitrile (FMDPA). Mp 199−200 °C. ATR-IR (neat, cm^{-1}) 2219 (s, C≡N str). ^1H NMR (DMSO-d_6): 7.09−7.15 (m, 7 H), 7.32−7.38 (m, 5H), 7.54−7.58 (t, 1H, J = 16 Hz, J' = 8 Hz), 7.68−7.72 (t, 2H, J = 16 Hz, J' = 8 Hz), 7.92 (s, 1H), 8.13−8.15 (d, 1H, J = 8 Hz). ^1H NMR (400 MHz, $CDCl_3$): 7.09−7.16 (m, 7 H), 7.18−7.22 (td, 1H, J = 16 Hz, J' = 8 Hz, J'' = 1.2 Hz), 7.29−7.35 (m, 5H), 7.40−7.45 (m, 2H), 8.06 (d, 1H, J = 1.6 Hz), 8.28−8.29 (d, 1H, J = 8 Hz). MS (FAB): found m/z = 395.14180; calcd for $C_{28}H_{17}N_3$, m/z = 395.14170.

2-(1-Carbazolyl)-fluoren-9-ylidene Malononitrile (FMCz). Mp >260 °C. ATR-IR (neat, cm^{-1}) 2224 (s, C≡N str). ^1H NMR (DMSO-d_6) 7.32−7.36 (t, 2H, J = 16 Hz, J' = 8 Hz), 7.46−7.55 (m, 5H), 7.70−7.74 (t, 1H, J = 16 Hz, J' = 8 Hz), 7.94−7.96 (dd, 1H, J = 8 Hz, J' = 1.2 Hz), 8.02−8.04 (dd, 1H, J = 8 Hz, J' = 0.4 Hz), 8.18−8.20 (d, 1H, J = 8 Hz), 8.28−8.31 (t, 3H, J = 12 Hz, J' = 8 Hz), 8.45 (s, 1H). MS (FAB): found m/z = 393.12562; calcd for $C_{28}H_{15}N_3$, m/z = 393.12605.

2-(N,N-Dianisylamino)-fluoren-9-ylidene Malononitrile (FMDAA). Mp 182−184 °C. ATR-IR (neat, cm^{-1}) 2224 (s, C≡N str). ^1H NMR (DMSO-d_6): 3.75 (s, 6 H), 6.85−6.88 (dd, 1H, J = 8 Hz, J' = 2 Hz), 6.94−6.96 (d, 4H, J = 8 Hz), 7.09−7.11 (d, 4H, J = 8 Hz), 7.26−7.30 (t, 1H, J = 16 Hz, J' = 8 Hz), 7.50−7.54 (t, 1H, J = 16 Hz, J' = 8 Hz), 7.56−7.58 (d, 1H, J = 8 Hz), 7.62−7.63 (d, 1H, J = 2 Hz), 7.77 (d, 1H, J = 8 Hz), 8.09−8.11 (d, 1H, J = 8 Hz). MS (FAB): found m/z = 455.1634; calcd for $C_{30}H_{21}N_3O_2$, m/z = 455.16283.

2-(N-Anisylamino)-fluoren-9-one (FOAA). Mp 152−154 °C. ATR-IR (neat, cm^{-1}) 3355 (N−H str), 1704 (s, C═O str). ^1H NMR (400 MHz, DMSO-d_6): 3.74 (s, 3 H), 6.92−6.96 (d, 2H, J = 8 Hz), 7.00−7.02 (dd, 1H, J = 8 Hz, J' = 1.6 Hz), 7.06−7.10 (m, 3H), 7.17−7.21 (t, 1H, J = 8 Hz), 7.47−7.56 (m, 4H), 8.31 (s, 1H). MS (FAB): found m/z = 301.3; calcd for $C_{20}H_{15}NO_2$, m/z = 301.1. HR-MS (ESI): found m/z = 302.1171 (M + H); calcd for $C_{20}H_{15}NO_2$, m/z = 301.11028.

2(N-Anisylamino)-fluoren-9-ylidene Malononitrile (FMAA). Mp 187−188 °C. ATR-IR (neat, cm^{-1}) 3337 (N−H str), 2222 (sh, C≡N str). ^1H NMR (400 MHz, DMSO-d_6): 3.73 (s, 3 H), 6.89−6.91 (d, 2H, J = 8 Hz), 7.01−7.03 (dd, 1H, J = 8 Hz, J' = 2 Hz), 7.09−7.11 (d, 2H, J = 8 Hz), 7.22−7.26 (t, 1H, J = 8 Hz), 7.47−7.51 (t, 1H, J = 8 Hz), 7.55−7.59 (t, 2H, J = 8 Hz), 7.89 (dd, 1H, J = 2 Hz), 8.08−8.10 (d, 1H, J = 8 Hz), 8.49 (s, 1H). MS (FAB): found m/z = 349.4; calcd for $C_{23}H_{15}N_3O$, m/z = 349.1. HR-MS (ESI): found m/z = 372.1087 (M + Na); calcd for $C_{23}H_{15}N_3O$, m/z = 349.12151.

2-(N,N-Dianisylamino)-7-(3,4,5-trimethoxyphenyl-2-ethenyl)-fluoren-9-ylidene Malononitrile (FMDAAS). Does not melt. ATR-IR (neat, cm^{-1}) 2222 (s, C≡N str). ^1H NMR (400 MHz, DMSO-d_6): 3.67 (s, 3 H), 3.75 (s, 6 H), 3.83 (s, 6 H), 6.85−6.87 (dd, 1 H, J = 8 Hz, J' = 2 Hz), 6.92−6.96 (m, 6 H), 7.08−7.11 (m, 5 H), 7.22−7.26 (d, 1 H, J = 16 Hz), 7.55−7.57 (d, 1 H, J = 8 Hz), 7.62−7.64 (d, 1 H, J = 8 Hz), 7.75−7.77 (dd, 2 H, J = 8 Hz, J' = 1.6 Hz), 8.24 (s, 1 H). MS (FAB): found m/z = 647.2413; calcd for $C_{41}H_{33}N_3O_5$, m/z = 647.24202.

2,7-Bis(N-Anisylamino)-fluoren-9-one Malononitrile (FOBAA). Mp 214−216 °C. ATR-IR (neat, cm^{-1}) 3329−3394 (N−H str), 1714 (s, C═O str). ^1H NMR (400 MHz, DMSO-d_6): 3.74 (s, 3 H), 6.92−6.96 (d, 2H, J = 8 Hz), 7.00−7.02 (dd, 1H, J = 8 Hz, J' = 1.6 Hz), 7.06−7.10 (m, 3H), 7.17−7.21 (t, 1H, J = 8 Hz), 7.47−7.56 (m, 4H), 8.31 (s, 1H). HR-MS (ESI): found m/z = 422.1596; calcd for $C_{27}H_{22}N_2O_3$, m/z = 422.16304.

2,7-Bis(N-Anisylamino)-fluoren-9-ylidene Malononitrile (FMBAA). Mp 204−205 °C. ATR-IR (neat, cm^{-1}) 3344 (N−H str), 2225 (sh, C≡N str). ^1H NMR (400 MHz, DMSO-d_6): 3.72 (s, 6 H), 6.86−6.88 (d, 4H, J = 8 Hz), 6.94−6.96 (dd, 2H, J = 8 Hz, J' = 1.6 Hz), 7.04−7.06 (d, 4H, J = 8 Hz), 7.30−7.32 (d, 2H, J = 8 Hz), 7.80−7.81 (d, 2H, J = 1.6 Hz), 8.26 (s, 2H). MS (FAB): found m/z = 470.2; calcd for $C_{30}H_{22}N_4O_2$, m/z = 470.2. HR-MS (ESI): found m/z = 471.1793 (M + H); calcd for $C_{30}H_{22}N_4O_2$, m/z = 470.17428.

2,7-Bis(N,N-Dianisylamino)-fluoren-9-ylidene Malononitrile (FMBDAA). Mp 106−108 °C. ATR-IR (neat, cm^{-1}) 2221 (s, C≡N str). ^1H NMR (400 MHz, DMSO-d_6): 3.73 (s, 12 H), 6.81−6.83 (dd, 2H, J = 8 Hz, J' = 2 Hz), 6.91−6.93 (d, 8H), 7.03−7.05 (d, 8H, J = 8 Hz), 7.34−7.36 (d, 2H, J = 8 Hz), 7.68−7.69 (d, 2H, J = 2 Hz). MS (FAB): found m/z = 682.2580; calcd for $C_{44}H_{34}N_4O_4$, m/z = 682.25746.

3,6-Bis(N,N-Dianisylamino)-fluoren-9-one (FOBDAA36). Mp 119−120 °C. ATR-IR (neat, cm^{-1}) 1684 (s, C═O str). ^1H NMR (400 MHz, DMSO-d_6): 3.75 (s, 12 H), 6.42−6.44 (dd, 2H, J = 8 Hz, J' = 2 Hz), 6.58−6.59 (d, 2H, J = 1.6 Hz), 6.94−6.96 (d, 8H, J = 8 Hz), 7.12−7.14 (d, 8H, J = 8 Hz), 7.30−7.32 (d, 2H, J = 8 Hz). MS (FAB): found m/z = 634.2455; calcd for $C_{41}H_{34}N_2O_5$, m/z = 634.24622.

3,6-Bis(N,N-Dianisylamino)-fluoren-9-ylidene Malononitrile (FMBDAA36). Mp 178−180 °C. ATR-IR (neat, cm^{-1}) 2212 (s, C≡N str). ^1H NMR (400 MHz, DMSO-d_6): 3.76 (s, 12 H), 6.48−6.51 (dd, 2H, J = 8 Hz, J' = 2 Hz), 6.54−6.55 (d, 2H, J = 1.6 Hz), 6.96−6.98 (d, 8H, J = 8 Hz), 7.16−7.18 (d, 8H, J = 8 Hz), 7.90−7.92 (d, 2H, J = 8 Hz). MS (FAB): found m/z = 682.2580; calcd for $C_{44}H_{34}N_4O_4$, m/z = 682.25746.

Electrochemical Measurements. Cyclic voltammetry was obtained at a scan rate of 150 mV/s using a BASi Epsilon Electrochemical Workstation equipped with platinum auxiliary and working electrodes and an Ag/AgCl reference electrode using tetrabutylammonium hexafluorophosphate as conducting electrolyte. Ferrocene oxidation was used as an external standard. The first oxidation onset voltages were used to estimate[9] HOMO energy levels (E_{HOMO}) for all compounds using eq 1. The spectral optical transition energies (E_g) in electron volts from the lowest-energy absorption peak onsets in acetonitrile were then used to estimate E_{LUMO} using eq 2. For compounds FO and FM, *both* E_{HOMO} and E_{LUMO} were obtained from voltammetric oxidation−reduction onsets using eq 1.

$$E_{MO} = -(E_{redox} + 4.8)\ \text{eV} \quad (1)$$

$$E_{LUMO} = E_{HOMO} + E_g \quad (2)$$

Computational Methods. All computations were carried out using Gaussian 09[10] revision B.01 on a Linux computer running openSuSE. Molecular geometries were optimized at a B3LYP[11]/6-31G(d,p) level, and these geometries were fixed to compute molecular properties at a B3LYP/6-31+G(d,p) level. Molecular orbital diagrams were generated from the final

checkpoint files using GaussView[12] version 5.0.9 with default parameter settings unless otherwise stated.

RESULTS

Subsequent discussions use the abbreviations shown in Scheme 1 for the structural modules used to make the donor–acceptor molecules of Scheme 2. As mentioned earlier, for analogous structures with the same donor units the LUMO level of an FO-based molecule will be lowered in the analogous FM-based system. The results described below show that this approach works well to give a range of absorption profiles and electronic HOMO and LUMO levels.

Scheme 1. General Structural Design Units Used in Donor–Acceptor Fluoren-9-ylidene Malononitrile (FM) and Precursor Fluorenone (FO) Systems in This Study

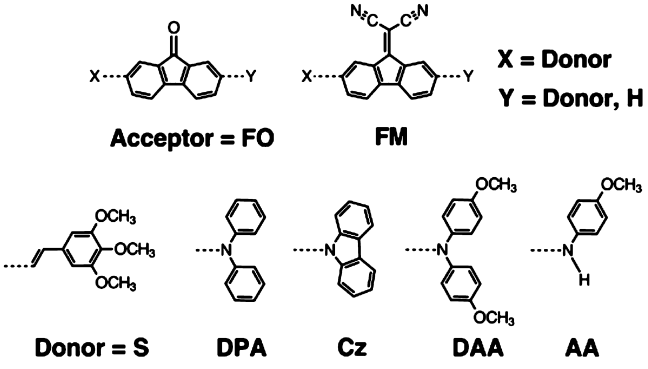

Energy Levels of Electronic Donor and Acceptor Structural Modules. The spectroscopic behaviors of all of the donor–acceptor systems in this study are interpreted below in terms of interactions between the donor (D) and acceptor (A) modules that comprise the overall D–A and D–A–D molecules. These interpretations are, in turn, related to HOMO and LUMO levels estimated from eqs 1 and 2 from the Electrochemical Measurements section. Therefore, each of the building block modules from Scheme 1 was electrochemically evaluated. Table 1 lists the "building block" electrochemical potentials for use in subsequent discussions, and individual cyclic voltammograms are given in Supporting Information (Figure S1). The individual donor modules trimethoxystyrene (S), carbazole (Cz), diphenylamine (DPA), and anisylamine (AA) each show one irreversible oxidation feature. Dianisylamine (DAA) shows well-differentiated oxidation onsets at 140, 783, and 1620 mV: the lowest potential oxidation is highly reversible and attributable to formation of the aminium radical cation, while the quasi-reversible second oxidation is attributable to diarylaminium oxidation. Neither of the acceptor modules FO or FM shows oxidation onset below 1500 mV, so oxidation features in the donor–acceptor molecules at lower potentials can confidently be attributed to donor module electrochemistry. FO shows a quasi-reversible reduction onset at −1820 mV, and FM shows reversible first and second reduction onsets at −1010 mV and−1710 mV,

Scheme 2. Donor–Acceptor Systems Compared in This Study

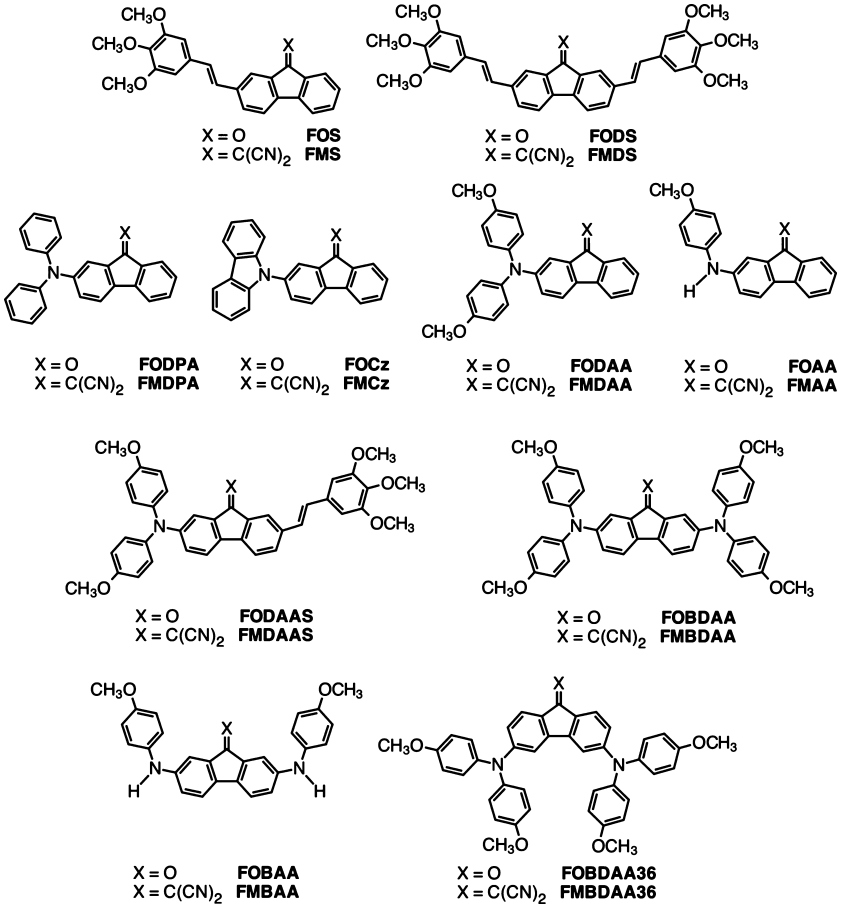

dx.doi.org/10.1021/jp407854r | J. Phys. Chem. A 2014, 118, 475–486

Table 1. Optical and Electrochemical Properties of Donor–Acceptor Molecules

compound	absorption λ_{max} (nm)[a] (ε = log{L/[mol−cm]}) low polarity	absorption λ_{max} (nm)[b] (ε = L/[mol−cm]) high polarity	oxidation onset(s) (mV[d])	reduction onset(s) (mV[d])	HOMO energy (eV)[e] expt [computed[f]]	LUMO energy (eV)[e] expt [computed[f]]
FOS	302(4.45), 348(4.45) 433(3.27)	307(4.49), 347(4.49), 441(3.26)	594	[c]	−5.39 [−5.61]	−2.98 [−2.59]
FMS	331(4.64) 547 (2.93)[g]	330(4.77), 539(2.84)	591	−817, −1612	−5.39 [−5.72]	−3.49 [−3.46]
FODS	306(4.50), 360(4.55), 454(3.63)	312(4.60), 370(4.75), 474(3.65)	556	−1430	−5.36 [−5.40]	−3.12 [−2.61]
FMDS	345(4.86), 373(4.77), 608(3.24)[g]	340(4.86), 366(4.81), 589(3.21)	642	−1090, −1720	−5.44 [−5.50]	−3.71 [−3.44]
FOCz	255(4.35), 290 (4.34) 430(2.87)	253(4.71), 290(4.31), 432(2.73)	715	−1490	−5.51 [−5.73]	−3.05 [−2.80]
FMCz	317(4.33), 340(4.28), 537(2.61)[h]	310(4.52), 338(4.44), 520(2.62)	484, 859	−1140	−5.28 [−5.83]	−3.35 [−3.66]
FODPA	295(4.47), 354(4.26), 479(3.19)	296(4.50), 350(4.20), 496(3.08)	320, 824	−1370	−5.12 [−5.37]	−3.01 [−2.54]
FMDPA	289(4.02), 325(4.20), 627(2.63)	324(4.35), 635(2.76)	517, 1280	−966, −1700	−5.32 [−5.51]	−3.73 [−3.42]
FOAA	288(4.51), 344(4.20), 498(3.05)[h]	289(4.48), 344(4.13), 505(2.96)	350, 838	−1660	−5.15 [−5.32]	−3.07 [−2.44]
FMAA	(insoluble in multiple solvents)	314(4.61), 342(4.35,sh), 649(2.73)	438, 984	−970, −1650	−5.24 [−5.53]	−3.72 [−3.38]
FODAA	295(4.45), 357(4.21), 502(3.22)	294(4.48), 350(4.16), 518(3.11)	232, 816	−1980	−5.03 [−5.05]	−3.02 [−2.41]
FMDAA	212(4.72), 323(4.44), 677(2.96)	323(4.37), 672(2.90)	220, 835	−1290, −1490, −1820	−5.02 [−5.19]	−3.55 [−3.30]
FODAAS	298 (4.55) 386 (4.50) 524 (3.52)	306(4.62), 384(4.64), 543(3.43)	178, 667, 893	−1590	−4.98 [−4.97]	−3.05 [−2.40]
FMDAAS	342(4.58), 397(4.39), 730(2.94)[g]	370(4.50), 389(4.51), 710(2.98)	229, 688, 962	−959, −1670	−5.03 [−5.31[j]]	−3.63 [−3.51[j]]
FOBDAA	298(4.57), 382(4.46), 554(3.25)	298(4.72), 376(4.58), 586(3.24)	155, 355, 949	−1410	−4.95 [−4.72]	−3.21 [−2.28]
FMBDAA	388(4.36), 522(2.05), 788(2.74)[h]	373(4.33), 531(2.46), 785(2.73)	176, 401, 943	−1170, −1760	−4.98 [−4.83]	−3.77 [−3.14]
FOBAA	295(4.64), 360(4.52), 559(3.11)	296(4.68), 359(4.53), 571(3.07)	157, 412	−1660	−4.96 [−4.91]	−3.13 [−2.33]
FMBAA	(insoluble in multiple solvents)	354(4.38,sh), 450(2.41,sh), 762(2.68)	243, 543, 1160	−952, −1610	−5.04 [−5.06]	−3.78 [−3.24]
FOBDAA36	334(4.28), 388(4.17), 463(4.07)[h]	327(4.28), 380(4.15), 474(4.02)	290(424, 533)[i]	−959, (−1127)[i]	−5.09 [−4.99]	−2.86 [−2.01]
FMBDAA36	359(3.84), 488(4.03), 585(3.70][h]	347(3.80), 483(3.97), 597(3.64)	279 (437, 572)[i]	−1060, −1730(−1230, −1850)[i]	−5.08 [−5.24]	−3.32 [−2.79]
S			637	[c]	−5.44 [−5.87]	−1.51 [−1.11]
Cz			810	[c]	−5.61 [−5.78]	−2.00 [−1.09]
DPA			440	[c]	−5.25 [−5.42]	−1.34 [−0.63]
AA			190	[c]	−4.99 [−5.31]	−1.29 [−0.34]
DAA			140, 783, 1620	[c]	−4.94 [−4.92]	−1.38 [−0.48]
FO			1550	−1820	−6.35 [−6.56]	−2.98 [−2.63]
FM			1500	−1010, −1710	−6.36 [−6.87]	−3.79 [−3.55]

[a]Three lowest-energy maxima; hexane solvent unless otherwise stated. All results obtained in acetonitrile, and referenced against ferrocene/ferrocenium oxidation in the same solvent. [b]Up to three lowest-energy maxima above 250 nm; acetonitrile solvent unless otherwise stated. All results obtained in acetonitrile, and referenced against ferrocene/ferrocenium oxidation in the same solvent. [c]No resolvable feature. [d]Onset potentials in millivolts. All results obtained in acetonitrile, and referenced against ferrocene/ferrocenium oxidation in the same solvent. [e]Calculated using eqs 1 and 2. [f]Computed at the B3LYP/6-31+G(d,p)//B3LYP/6-31G(d,p) level of theory unless otherwise stated. [g]Spectrum obtained in dichloromethane because of hexane insolubility. [h]Spectrum obtained in diethyl ether because of hexane insolubility. [i]Potential of peak maximum in millivolts. [j]Computed at the B3LYP/6-31G(d,p) // B3LYP/6-31G(d) level.

dx.doi.org/10.1021/jp407854r | J. Phys. Chem. A 2014, 118, 475−486

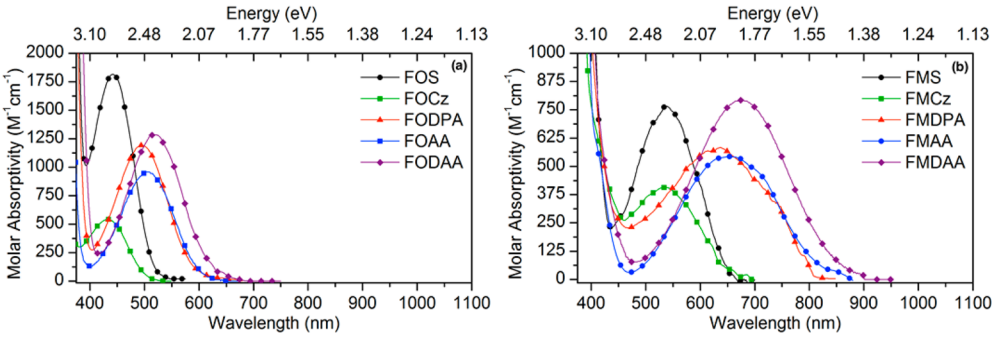

Figure 1. Lowest-energy absorption spectral regions in acetonitrile of fluorenones (a) and fluorenylidene malononitriles (b) with one donor substituent.

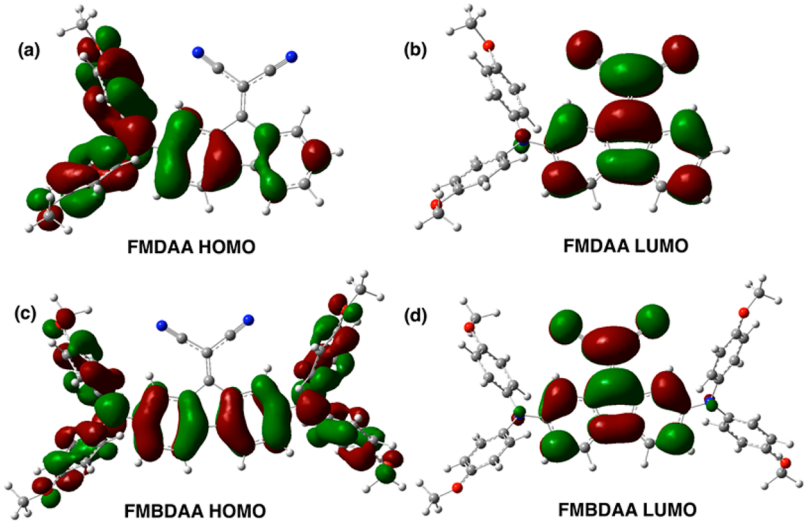

Figure 2. Example B3LYP/6-31+G(d,p) level frontier orbital plots for FMDAA HOMO (a) and LUMO (b) and FMBDAA HOMO (c) and LUMO (d). Plotted using default parameters for GaussView version 5.0.9.

respectively; the features in the stronger acceptor-substituent FM are well-defined and reversible.

Monosubstituted D−A Type Donor−Acceptor Systems. Table 1 summarizes major solution UV−vis−NIR spectral features for the monosubstituted, donor−acceptor (D−A) FOs and FMs whose structures are given in Scheme 2: full-range spectra over 200−900 nm are given in Supporting Information (Figures S2−S3). All of the FO-based compounds have multiple strong transitions between 250 and 380 nm with molar absorptivities ranging over 9 000−60 000 M^{-1} cm^{-1}, but mostly ∼30,000 M^{-1} cm^{-1}. The FM-based systems exhibit overlapping bands at 300−380 nm with more variable molar absorptivities of 18 000−60 000 M^{-1} cm^{-1}. With minor variations in position, and somewhat greater variations in intensity, these stronger bands are seen in the absorption spectra of all of the Scheme 2 compounds, except for the FM systems with 3,6-connectivity. This will be discussed below.

Figure 1 shows the lowest-energy absorption band regions of the monosubstituted systems. The FO-based systems show absorption onset at 500−650 nm, with molar absorptivities of about 500−1800 M^{-1} cm^{-1}. The FM-based systems are red-shifted by comparison to their FO-based structural analogues, with absorption onset at about 650−900 nm, and molar absorptivities of about 400−800 M^{-1} cm^{-1}. Despite their modest molar absorptivities by comparison to the main transitions below 400 nm, these long wavelength bands impart strong colors to the neat solids and in sufficiently concentrated solutions, ranging from red to blue-black.

The FO- and FM-based systems functionalized with trimethoxystyrene, FOS and FMS, exhibit the highest-energy absorption onsets, along with the *N*-carbazolyl (Cz) functionalized systems. The longer π-system conjugation in FOS and FMS gives larger molar absorptivities compared to the systems monosubstituted by amines, but the relatively high-energy absorption onsets show the styrene unit to be less effective as an electron donor than the noncarbazolyl amines tested in this study.

The FOS long wavelength absorption band red shifts in polar solvents, a trend typically attributed to $\pi\rightarrow\pi^*$ transitions. These and other solvatochromic shifts are summarized in Supporting Information (Table S1). Interestingly, the FMS long wavelength band exhibits a modest blue shift in acetonitrile versus less polar solvents, as do a number of the Scheme 2 FM-based derivatives described below. Such behavior can be attributed to $n\rightarrow\pi^*$ transitions, but computational modeling shows the frontier orbitals of the Scheme 1 compounds to be π-orbitals, without interspersed n-type orbitals. The long wavelength transitions in both FO- and FM-based systems are all computed to be $\pi\rightarrow\pi^*$ type, from a π-HOMO that is delocalized throughout the full π-system to a LUMO that is largely localized on the FO or FM unit. Examples are shown in Figure 2 for both D−A and D−A−D systems; all of the frontier MOs are shown in the Supporting Information (Summary S1).

dx.doi.org/10.1021/jp407854r | J. Phys. Chem. A 2014, 118, 475−486

Conformational differences in the AA donor-substituted systems show only small differences in computed MO energy levels (≤0.1 eV). As the electron donor strength of donor modules increases, the HOMO and LUMO overlap less, with the HOMO primarily on the donor module and the LUMO primarily on the acceptor unit. This is conducive to intramolecular charge transfer (ICT) character in the lowest-energy photoexcitation. Negative solvatochromic shifts in polar, n-donor type solvents (like the acetonitrile used in the present study) can be attributed[13] to specific solvent−solute interactions in the ground state that are less favorable for the excited state, giving a net blue shift; this behavior can occur for both CT and n→π^* transitions. For this reason, the blue shift seen in acetonitrile versus lower-polarity solvents for FMS and a number of other malononitrile derivatives in this study is reasonable for excited states having the significant ICT character indicated by our computations.

To evaluate the frontier orbital energetics of FOS and FMS and the related amine-substituted D−A compounds, their solution electrochemistry was studied. Cyclic voltammetry shows an oxidation potential for trimethoxystyrene that is much higher than for any of the amines except Cz, showing trimethoxystyrene to be a reluctant electron donor despite extending conjugation at the 2-position of FO or FM. FOS and FMS show only poorly resolved oxidation features with onsets similar to but somewhat lower in voltage than trimethoxystyrene, probably because of conjugation into the biphenyl-type π-system of FO and FM. FOS also shows no clear reduction feature, but the more strongly electron acceptor-substituted FMS shows quasi-reversible reduction features similar to (though weaker than) those for the FM group. Converting the FO to the FM group is so electron withdrawing that oxidation of the trimethoxystyrene unit becomes ineffective.

For the D−A systems bearing only one arylamine substituent, voltammetric features can be readily identified from reduction of the FO and FM units in each series of molecules. FODAA shows reversible first oxidation and second oxidation features (232 and 816 mV) that can be associated with the electron-rich DAA group; FOAA also shows reversible first and second oxidation features (350 and 838 mV) that can be attributed to the electron-rich AA group, indicating that even one anisyl group is sufficient to stabilize oxidation to the FOAA aminium species. Similarly, FODPA and FOCz show quasi-reversible oxidation features that are analogous to features in DPA and Cz. Strong electron withdrawing substitution on the FM-based systems stabilizes the reduction electrochemistry by comparison, giving clear and reversible FM-associated reduction features in FMCz, FMDPA, and FMAA, and somewhat less so but still readily identified reduction in FMDAA. But, no FMCz, FMDPA, or FMDAA oxidation features are strong or clearly reversible (FMAA oxidation is quasi-reversible); the poor reversibility is consistent with destabilization of oxidation by the strongly electron-withdrawing FM module.

Experimentally, the FO systems all show solvatochromic red shifts of the lowest-energy transition in more polar solvents, consistent with $\pi\rightarrow\pi^*$ and ICT character for these transitions.[14] The solvatochromic trends for the FM systems are not completely consistent but somewhat favor blue shifts in more polar solvents, like the case of the FMS versus FOS. Figure 3 shows the long wavelength regions of the spectra for FODAA and FMDAA in diethyl ether and acetonitrile, with full scale spectra given in Supporting Information (Figure S5); tabular results for all solvatochromic experiments are given in Supporting Information (Table S1). As mentioned above, the blue shifts in some of the FM systems are attributable[13] to specific solvent−solute interactions in acetonitrile solvent.

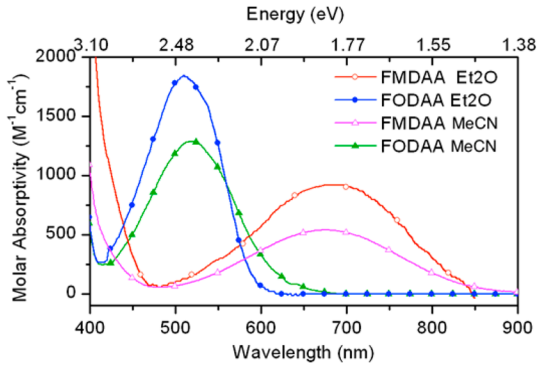

Figure 3. Comparison of lowest-energy absorption spectral regions for FODAA and FMDAA in diethyl ether (Et2O) and acetonitrile (MeCN).

Interestingly, the band onsets for the Cz-functionalized D−A systems are nearly the same as those for the trimethoxystyrene-functionalized systems. The pyrrole ring of Cz is less able to donate aromatic π-electrons than the other amine donors are able to donate nonaromatic lone pair electrons. This makes Cz a relatively poor donor, resulting in a relatively higher optical transition energy. Also, the relatively lower oxidation potential and higher computed HOMO energy of trimethoxystyrene (Table 1) indicate it to be a superior electron donor to Cz. For the stronger donor amines, the absorption onsets in Figure 1 move to increasingly lower energy in the series FOCz > FODPA > FOAA > FODAA. The decreasing optical transition energies correlate with increasing E_{HOMO} of Cz < DPA < AA < DAA, while E_{LUMO} in the FO-series remains fixed at about −3.0 eV, as shown experimentally by both electrochemical measurements and computational modeling. The same trend is seen for the FM-functionalized analogues, but in each case the FM-analogue absorption is lower in energy by about 0.50 eV. The reduced optical transition energies in the FM-series occur because their HOMO levels are essentially defined by the same donor HOMO levels as in their FO analogues, but the FM-analogues all have lower E_{LUMO} energies in the range of −3.4 to −3.7 eV (Table 1). The computations for all of the amine-functionalized D−A systems show an ICT character that is even stronger than that in FOS or FMS, with the π-HOMO in each case favoring the side of the FO or FM ring that holds the amine and the π^*-LUMO being localized on the FO or FM module.

Disubstituted D−A−D Donor−Acceptor Systems. The through-conjugated 2,7-FO and 2,7-FM systems show quite similar higher-energy absorption spectral features to those of the monosubstituted 2-FO and 2-FM analogues, with strong features at higher energy around 400 nm that overlap more thoroughly in the FM systems than in the FO systems. The low-energy bands >400 nm are shown in Figure 4, and the full scale 200−900 nm spectra are given in Supporting Information (Figures S2 and S4). The molar absorptivities for these disubstituted systems are higher than for the monosubstituted analogues, as expected. Solvatochromic effects parallel the behavior of the monosubstituted analogues for both FO- and FM-series disubstituted molecules (see Supporting Information, Table S1).

dx.doi.org/10.1021/jp407854r | J. Phys. Chem. A 2014, 118, 475−486

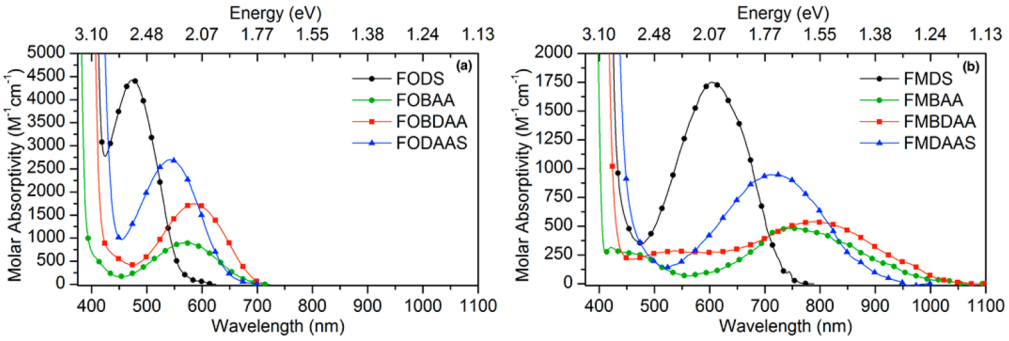

Figure 4. Lowest-energy absorption spectral regions in acetonitrile of fluorenones (a) and fluorenylidene malononitriles (b) with two donor substituents.

Scheme 3. Tuning of Donor–Acceptor System (D–A) Frontier Molecular Orbitals Derived from Interaction of Donors and Acceptors

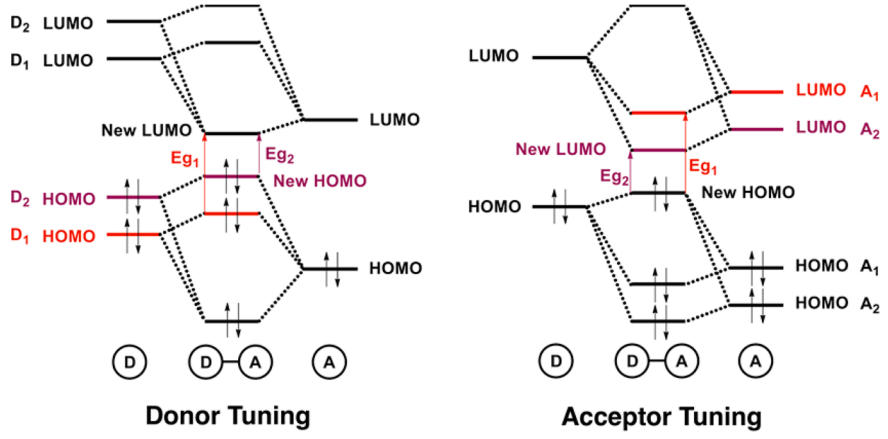

The increased effective conjugation achieved by placing two donor substituents in the 2,7-positions, with resonance connectivity between them, is most strongly seen in red-shifted low-energy bands by comparison to the monosubstituted systems and in reduced oxidation potentials with more oxidation features in the voltammograms. Although FODS and FMDS have the longest extended C=C type π-systems, the amine-substituted D–A–D systems give the largest optical transition energy decrease relative to the corresponding monosubstituted systems. The band onset for FMBDAA is at about 1000 nm (1.2 eV), in the NIR region: the neat solids appear black to the naked eye.

Comparing the monosubstituted to disubstituted systems allows some relative comparisons of substituent effects on the spectroscopy. FODAAS has an absorbance maximum at an energy that is 0.34 eV lower than that in FODS: the higher HOMO energy for the DAA group (Table 1) gives this lower bandgap because the LUMO levels are very similar for FODS and FODAAS. Similarly, FMDAAS has an absorbance maximum 0.36 eV lower than that of FMDS. Although FMDAAS has only one amine donor group, the combination of the DAA donor with the C=C conjugation extension of the trimethoxystyrene unit gives a low-energy band onset in acetonitrile of ~900 nm (1.4 eV).

The D–A–D systems with the strongest donor substitution, FOBDAA and FMBDAA, show the electrochemical features of both their constituent donor (DAA) *and* acceptor modules. FOBDAA shows reduction consistent with FO at −1410 mV, and FMBDAA at −1170 and −1760 mV is consistent with FM. Both show a closely spaced pair of oxidation features attributable to the two DAA groups in each. From the Table 1 data, the two lowest oxidation onset potentials are split by 200 and 225 mV for FOBDAA and FMBDAA, respectively; the analogous splittings for FOBAA and FMBAA are 255 and 300 mV, respectively. The splittings in both sets of diamines in the FM systems are larger than those in the FO systems. Increased splitting indicates a strong influence of the first redox center on the second, indicating stronger 2,7-through-conjugation interaction between amines in the FM system.[15] The larger splitting in bis-AA versus bis-DAA systems may be due to greater planarity and better through-conjugation in the sterically less hindered bis-AA systems. Finally, FODAAS with two different donor groups exhibits two oxidation features attributable to the DAA group (178 mV and 893 mV), plus an onset feature at 667 mV from trimethoxystyrene. FMDAAS shows three oxidation features analogous to those in FODAAS.

Modular Electronic Analysis of the Donor–Acceptor Molecules. The electrochemical findings support two criteria for a modular scheme for understanding the electronic behavior of the donor–acceptor molecules in this study. First, the molecules exhibit reduction electrochemistry in very reasonable accord with voltammetry measured for the FO and FM acceptor modules; there are only minor variations with different attached donor groups. (The reduction half-wave potentials also compare well to the FM reduction potential of −1.00 V from Neckers and co-workers[5b]). Second, the oxidation potentials of donor components are well-retained in both FO- and FM-based systems. These trends encourage the notion

dx.doi.org/10.1021/jp407854r | J. Phys. Chem. A 2014, 118, 475–486

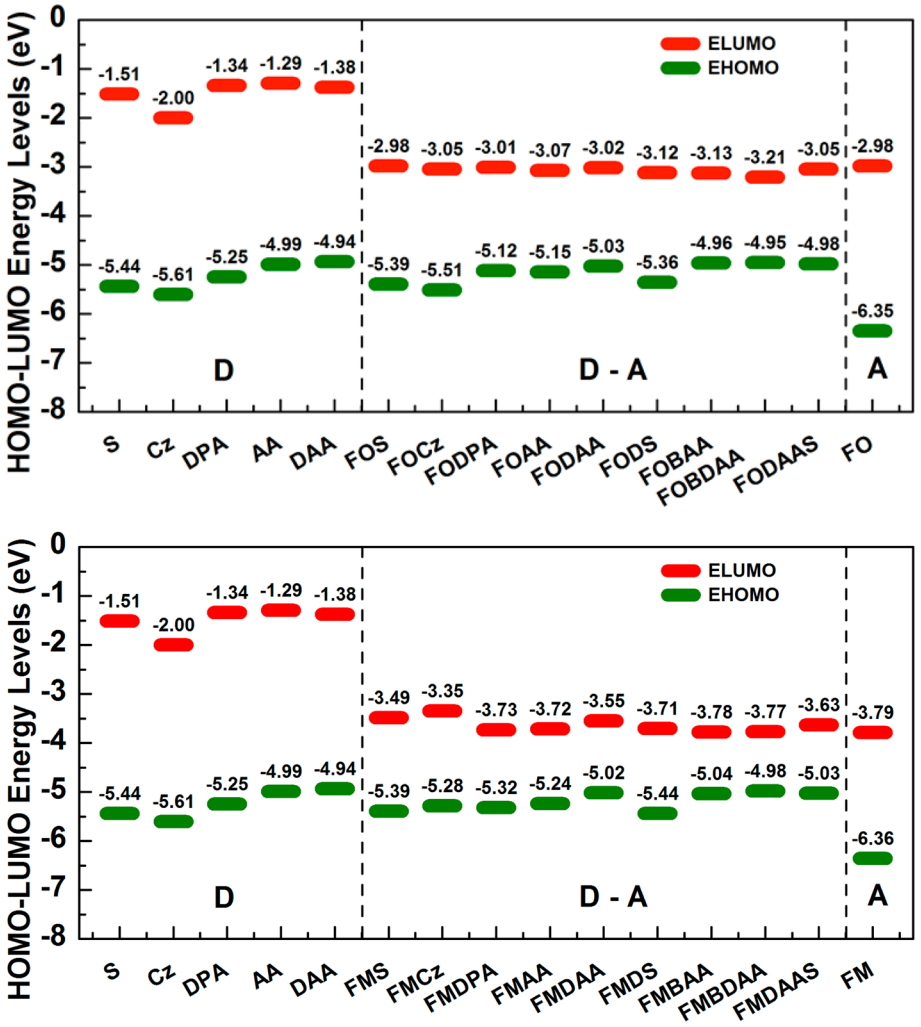

Figure 5. Frontier molecular orbital energy levels for donor–acceptor molecules compared with orbital energies of constituent donor and acceptor modules (data from Table 1).

that the donor and acceptor components can be considered interchangeable modules that can be used to design and understand the electronic properties of the overall D–A molecules. From a molecular engineering perspective, this is very desirable for designing new electronic materials. In addition, as Table 1 shows, the HOMO energy levels computed by density functional theory for the Scheme 2 donor–acceptor molecules are remarkably close to the experimentally estimated HOMO levels, on average about 0.1 ± 0.2 eV lower (uncertainty is standard deviation); the computed LUMO energy levels are 0.4 ± 0.3 eV higher than those obtained from voltammetry experiments.

One can rationalize the behavior of related donor–acceptor systems composed of modular units (like those in Scheme 1) by using computational and/or experimental frontier energy levels for the modular units. Scheme 3 shows how qualitative interactions between the frontier orbitals of donor and acceptor units decreases the optical transition energy of a donor–acceptor system, where donor strength D2 > D1 *and/or* acceptor strength A2 > A1. In the present study, the FO and FM acceptor unit HOMO energies are low enough not to interact strongly with the donor units. Similarly, the donor unit LUMOs are so high in energy relative to the acceptor LUMOs that the donor–acceptor system LUMOs are determined by the FO or FM units. Figure 5 shows quantitatively how the experimental donor–acceptor frontier energy levels track with the energies of their modular components. The B3LYP computational modeling reproduces these trends with similar orbital energies.

Experimentally, the LUMO energy levels in the FM systems are lower by an average of 0.6 ± 0.1 eV in comparison to their FO-based analogues (uncertainty is standard deviation considering only the donor–acceptor systems, not the modular units). This correlates with the 0.8 eV LUMO energy decrease from FO to FM and with the optical transition energy decreases (Table 1) in FM derivatives compared to FO derivatives. Therefore, the modular approach of Scheme 3 applied in Figure 5 is self-consistent in describing the electronic behaviors of the Scheme 2 donor–acceptor molecules.

Strengthening Absorption by a Connectivity Change. The success of the Figure 5 modular donor–acceptor design strategy is somewhat diluted by the decreased molar absorptivities of the desirably low optical transition energies in both FO and FM series. For photovoltaic and photoconversion applications, strong absorption bands are desirable to allow use of thinner layers of electroactive material.

We therefore extrapolated from Figure 5, following work by Neckers and co-workers[5,16] that tested the effect of connectivity

dx.doi.org/10.1021/jp407854r | J. Phys. Chem. A 2014, 118, 475–486

Scheme 4. Neckers's Push–Pull FO- and FM-Based Systems with Phenylethynylene-Linked Donors[a]

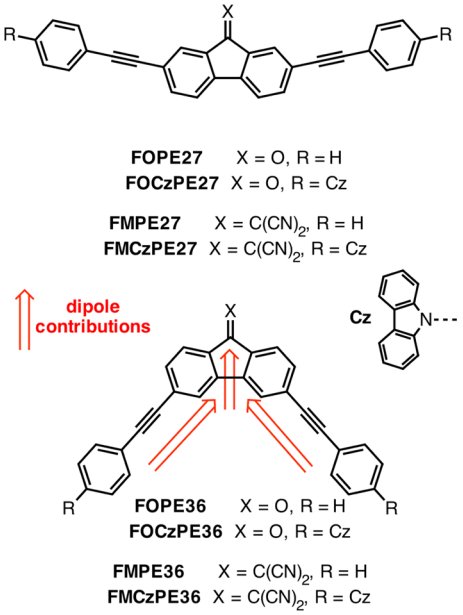

[a]Red arrows show dipole contributions in the 3,6-connectivity systems. Based on discussions from ref 16.

in the FO- and FM-based push–pull molecules shown in Scheme 4. They found that the absorption spectral blue shift from deconjugating the donor substituents in the 3,6-FO/FM systems (FOPE36, etc.) by comparison to the through-conjugated 2,7-FO/FM systems (FOPE27, etc.) was accompanied by a substantially *increased* molar absorptivity. In the 2,7-connectivity systems, excited-state dipole shift effects through the phenylethynyl groups cannot interact directly with the C═O or C═C(CN)$_2$ dipoles. In the 3,6-connectivity systems, the donor substituents are no longer through-conjugated with one another, but they are linked to the C═O or C═C(CN)$_2$ units. This gives higher optical transition energies, but reinforces excited-state dipole moment changes for donor Cz groups interacting with C═O or C═C(CN)$_2$ dipoles.

An analogous dipole enhancement was tested using the modules from Scheme 1. Computational modeling of FOBDAA and FMBDAA with time-dependent density functional (TDDFT[17]) methods at the B3LYP/6-31G(d,p) level gave long wavelength bands at 625 and 1042 nm, with oscillator strengths of 0.09 and 0.04, respectively (see Supporting Information, Table S2). The predicted band positions are good matches to the observed band onsets (Table 1), and the computed decrease in oscillator strength from the FO- to the FM-based system agrees with experiment. By comparison, the isomeric FOBDAA36 and FMBDAA36 were predicted to have long wavelength bands at 490 and 616 nm, with oscillator strengths of 0.23 and 0.24, respectively. However, save for different orbital energies due to different connectivities, the 2,7- and 3,6-systems both have similar push–pull separation in HOMO versus LUMO, indicating ICT (or at least strongly dipolar) character to be expected for transitions in both systems. These computations supported the use of Neckers's connectivity change strategy to increase absorptivity and indicated that FMBDAA36 would absorb well into the visible spectrum despite deconjugation of the donor groups from one another.

Accordingly, FOBDAA36 and FMBDAA36 were made by methods similar to those used for the other systems in this study. Their absorption spectra in acetonitrile are shown in Figure 6, and their cyclic voltammetric redox potentials given in

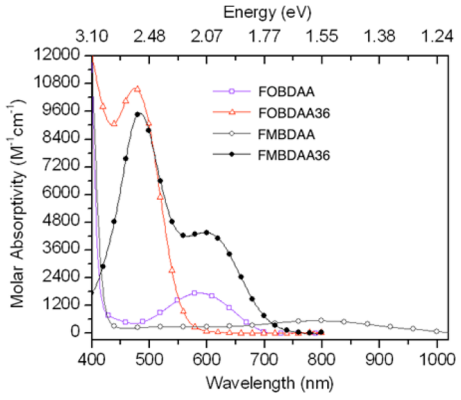

Figure 6. Lowest-energy absorption spectral regions in acetonitrile comparing FOBDAA, FMBDAA, FOBDAA36, and FMBDAA36.

Table 1; the full voltammograms are given in Supporting Information (Figure S7). Although feature onsets are given in Table 1 for consistent use with eqs 1 and 2, oxidation potential *maxima* are compared here because they are more precisely resolved in the voltammograms. The oxidation potential maxima were 424 and 553 mV for FOBDAA36 and 437 and 572 mV for FMBDAA36, compared to 268 and 444 mV for FOBDAA and 314 and 494 mV for FMBDAA. Not only are the oxidation potentials, and therefore the HOMO energies (see Table 1 and Supporting Information), raised significantly in the 3,6-isomers, but the splitting *between* oxidation features is decreased: 129 and 135 mV in the FO and FM systems compared to 176 and 180 mV in the 2,7-connectivity systems. Smaller splitting indicates a smaller interaction between amine units[18] in the 3,6-connectivity; this is as expected because there is no mutual oxidative stabilization by amine-to-amine resonance through direct 2,7-conjugation.

Figure 6 shows that the absorption band energies increase in the 3,6- versus the 2,7-connectivity systems, as expected. The observed absorption onsets in acetonitrile are at 0.3 ± 0.1 eV (standard deviation) higher energy than the TDDFT modeling predictions (see Supporting Information, Table S2), but the predicted and observed spectra both show the desired strong increases in molar absorptivity for both the FO- and FM-based systems. Overall, the combination of LUMO lowering by use of the FM unit plus increased dipole coupling in the 3,6-connectivity makes FMBDAA36 absorb 8-fold more strongly (molar absorptivity 4500 M^{-1} cm^{-1}) than any of the 2,7-connectivity systems. Also, FMBDAA36 still absorbs well into the 400–700 nm region that is important for organic photoconversion, making FMBDAA36 a good candidate for device testing. Recent work has shown other FO or FM derivatives to have promise for hole-transport or ambipolar charge transport,[19,20] where morphological considerations[21] do not curtail solid-state charge-transport behavior.

Figure 7 shows how the modular component frontier molecular orbitals compare to those of both the 2,7- and 3,6-connectivity systems. Notably, by this analysis the LUMO levels in the 3,6-systems are raised somewhat (relative to those

dx.doi.org/10.1021/jp407854r | J. Phys. Chem. A 2014, 118, 475–486

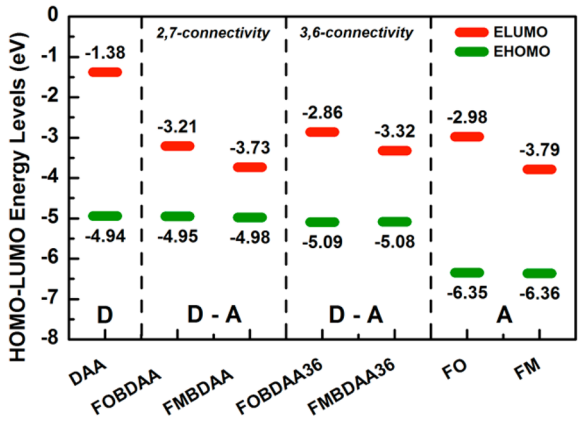

Figure 7. Frontier molecular orbital (FMO) energy levels for FOBDAA, FMBDAA, FOBDAA36, and FMBDAA36 compared to component FMO levels.

on the 2,7-connectivity system) by direct resonance interaction with the DAA donor groups, giving the observed increase in optical transition energies.

CONCLUSIONS

The absorption spectroscopy and electrochemistry of strong electron acceptor fluorenylidene malononitriles (FMs) bearing common 2- or 2,7- electron donor substituents were compared to the results for less electron withdrawing fluorenone (FO) analogues. The FM and FO units are structurally simple and synthetically accessible acceptor (A) units that interact with donor (D) substituents to give donor–acceptor electronic behavior, including longer wavelength optical transition energies associated with intramolecular charge transfer (ICT) behavior.

This modular electronic engineering approach provides a rational path for tuning E_{HOMO}, E_{LUMO}, optical transition energy, and absorptivity strength. Starting from FO-based systems bearing moderate donors such as trimethoxystyrene connected in a 2,7-fashion to maximize conjugation, stronger donor diarylamine substituents were used to raise HOMO levels, increasing ICT character and lowering the optical transition energy. Changing to a 3,6-connectivity strengthened molar absorptivity considerably, at a cost of increasing the optical transition energy by about 0.50 eV.

Molecular level electronic control is a necessary but insufficient criterion to produce desirable bulk electronic behavior. Because modest change in structure can give large changes in the solid-state morphologies that determine effective charge-transport properties, there is a continuing need to test many derivatives of electronically similar compounds to find the best molecular–morphological electronic property combinations. The present study exemplifies a strategy for rational testing of whole families of related molecules for potential electronic materials use, starting from electrochemical, spectroscopic, and computational evaluation of donor and acceptor components and using readily available molecular building blocks assembled in a few synthetic steps. Evaluation of these new materials for organic-based electronics is underway.

ASSOCIATED CONTENT

Supporting Information

Synthetic and characterization details, full scale absorption spectra for all compounds, and cyclic voltammograms for data summarized in Table 1; computational geometries; table of absorption energies and solvatochromic shifts in different solvents; TDDFT summaries for FOBDAA and FMBDAA isomers; and computational summaries with computed HOMO/LUMO pictures for all donor–acceptor systems. This material is available free of charge via the Internet at http://pubs.acs.org.

AUTHOR INFORMATION

Notes

The authors declare no competing financial interest.

ACKNOWLEDGMENTS

This work was supported as part of Polymer-Based Materials for Harvesting Solar Energy (PHaSE), an Energy Frontier Research Center funded by the U.S. Department of Energy, Office of Basic Energy Sciences under Award DE-SC0001087.

REFERENCES

(1) (a) Prasad, P. N.; Williams, D. J. *Introduction to Nonlinear Optical Effects in Molecules and Polymers*; Wiley: New York, 1991. (b) Zyss, J. *Molecular Nonlinear Optics: Materials, Physics and Devices*; Academic Press: Boston, 1993. (c) Kanis, D. R.; Ratner, M. A.; Marks, T. J. Design and Construction of Molecular Assemblies with Large Second-Order Optical Nonlinearities. Quantum Chemical Aspects. *Chem. Rev.* **1994**, *94*, 195–242. (d) Garnier, F. Organic-Based Electronics a la Carte. *Acc. Chem. Res.* **1999**, *32*, 209–217. (e) Segura, J. L.; Martin, N.; Guldi, D. M. Materials for Organic Solar Cells: the C60/π-Conjugated Oligomer Approach. *Chem. Soc. Rev.* **2005**, *34*, 31–47. (f) Jiang, H. Organic Ambipolar Conjugated Molecules for Electronics: Synthesis and Structure-Property Relationships. *Macromol. Rapid Commun.* **2010**, *31*, 2007–2034. (g) Organic Electronics–New Physical Chemistry Insight. Hu, W., Tao, Y.-T., Sirringhaus, H., Eds. *Phys. Chem. Chem. Phys.*, **2012**, *41*, 14081–14402.

(2) See, for example: (a) Patel, D. G.; Feng, F.; Ohnishi, Y.-y.; Abboud, K. A.; Hirata, S.; Schanze, K. S.; Reynolds, K. R. It Takes More Than an Imine: The Role of the Central Atom on the Electron-Accepting Ability of Benzotriazole and Benzothiadiazole Oligomers. *J. Am. Chem. Soc.* **2012**, *134*, 2599–2612. (b) Beaujuge, P. M.; Vasilyeva, S. V.; Liu, D. Y.; Ellinger, S.; McCarley, T. D.; Reynolds, J. R. Structure-Performance Correlations in Spray-Processable Green Dioxythiophene-Benzothiadiazole Donor-Acceptor Polymer Electrochromes. *Chem. Mater.* **2012**, *24*, 255–268. (c) Zhou, N.; Guo, X.; Ortiz, R. P.; Li, S.; Zhang, S.; Chang, R. P. H.; Facchetti, A.; Marks, T. J. Bithiophene Imide and Benzodithiophene Copolymers for Efficient Inverted Polymer Solar Cells. *Adv. Mater.* **2012**, *24*, 2242–2248. (d) Li, Y. Molecular Design of Photovoltaic Materials for Polymer Solar Cells: Electronic Energy Levels and Broad Absorption. *Acc. Chem. Res.* **2012**, *45*, 723–733. (e) Roncali, J. Linear π-Conjugated Systems Derivatized with C_{60}-Fullerene as Molecular Heterojunctions for Organic Photovoltaics. *Chem. Soc. Rev.* **2005**, *34*, 483–495. (f) Cheng, Y.-J.; Yang, S.-H.; Hsu, C.-S. Synthesis of Conjugated Polymers for Organic Solar Cell Applications. *Chem. Rev.* **2009**, *109*, 5868–5923. (g) Zhang, Z.-G.; Wang, J. Structures and Properties of Conjugated Donor-Acceptor Copolymers for Solar Cell Applications. *J. Mater. Chem.* **2012**, *22*, 4178–4187. (h) Zhou, H.; Yang, L.; You, W. Rational Design of High Performance Conjugated Polymers for Organic Solar Cells. *Macromolecules* **2012**, *45*, 607–632.

(3) (a) Kuboyama, A. Electronic Spectrum of Fluorenone. *Bull. Chem. Soc. Jpn.* **1964**, *37*, 1540–1544. (b) Kobayashi, T.; Nagakura, S. Picosecond Time-Resolved Spectroscopy and the Intersystem Crossing Rates of Anthrone and Fluorenone. *Chem. Phys. Lett.* **1976**, *43*,

429−434. (c) Andrews, L. J.; Deroulede, A.; Linschitz, H. Photophysical Processes in Fluorenone. *J. Phys. Chem.* **1978**, *82*, 2304−2309. (d) Yoshihara, K.; Kearns, D. R. Spectroscopic Properties of the Lower-Lying Excited States of Fluorenone. *J. Chem. Phys.* **1966**, *45*, 1991/1−9. (e) Arathi Rani, S.; Sobhanadri, J.; Prasada Rao, T. A. Determination of the Excited State Dipole Moment of Fluorenone using the Method of Solvatochromism. *Spectrochim. Acta, Part A* **1995**, *51*, 2473−2479. (f) Arathi Rani, S.; Sobhanadri, J.; Prasada Rao, T. A. Solvent and Concentration Effects on the Steady State Fluorescence of Fluorenone. *J. Photochem. Photobiol., A* **1996**, *94*, 1−5. (g) Murphy, R. S.; Moorlag, C. P.; Green, W. H.; Bohne, C. Photophysical Characterization of Fluorenone Derivatives. *J. Photochem. Photobiol., A* **1997**, *110*, 123−129.

(4) (a) Ferenczi, T. A. M.; Sims, M.; Bradley, D. D. C. On the Nature of the Fluorenone-Based Emission in Oxidized Poly(dialkyl-fluorene)s. *J. Phys.: Condens. Matter* **2008**, *20*, 045220/1−. (b) Sims, M.; Bradley, D. D. C.; Ariu, M.; Koeberg, M.; Asimakis, A.; Grell, M.; Lidzey, D. G. Understanding the Origin of the 535 nm Emission Band in Oxidized Poly(9,9-dioctylfluorene): The Essential Role of Inter-Chain/Inter-Segment Interactions. *Adv. Func. Mater.* **2004**, *14*, 765−781. (c) Kulkarni, A. P.; Kong, S.; Jenekhe, S. A. Fluorenone-Containing Polyfluorenes and Oligofluorenes: Photophysics, Origin of the Green Emission and Efficient Green Electroluminescence. *J. Phys. Chem. B* **2004**, *108*, 8689−8701. (d) Becker, K.; Lupton, J. M.; Feldmann, J.; Nehls, B. S.; Galbrecht, F.; Gao, D.; Scherf, U. On-chain Fluorenone Defect Emission from Single Polyfluorene Molecules in the Absence of Intermolecular Interactions. *Adv. Funct. Mater.* **2006**, *16*, 364−370. (e) Montilla, F.; Mallavia, R. On the Origin of Green Emission Bands in Fluorene-Based Conjugated Polymers. *Adv. Funct. Mater.* **2007**, *17*, 71−78. (f) Yang, G.-Z.; Wu, M.; Lu, S.; Wang, M.; Liu, T.; Huang, W. Thermooxidative Stability of Spectra of Fluorene-Based Copolymers. *Polymer* **2006**, *47*, 4816−4823.

(5) (a) Estrada, L. A.; Yarnell, J. E.; Neckers, D. C. Revisiting Fluorenone Photophysics via Dipolar Fluorenone Derivatives. *J. Phys. Chem. A* **2011**, *115*, 6366−6375. (b) Estrada, L. A.; Cai, X.; Neckers, D. C. Nonradiative Decay Mechanism of Fluoren-9-ylidene Malononitrile Ambipolar Derivatives. *J. Phys. Chem. A* **2011**, *115*, 2184−2195.

(6) (a) Eakins, G. L.; Alford, J. S.; Tiegs, B. J.; Breyfogle, B. E.; Stearman, C. J. Tuning HOMO-LUMO Levels: Trends Leading to the Design of 9-Fluorenone Scaffolds with Predictable Electronic and Optoelectronic Properties. *J. Phys. Org. Chem.* **2011**, *24*, 1119−112. (b) Shigeta, M.; Morita, M.; Konishi, G.-i. Selective Formation of Twisted Intramolecular Charge Transfer and Excimer Emissions on 2,7-Bis(4-diethylaminophenyl)-fluorenone by Choice of Solvent. *Molecules* **2012**, *17*, 4452−4459. (c) Nayak, M. K.; Dogra, S. K. Photophysics of 1-Hydroxy- and 1-Methoxy-9-fluorenone. *J. Photochem. Photobiol. A* **2005**, *169*, 299−307. (d) Heldt, J. R.; Heldt, J.; Jozefowicz, M.; Kaminski, J. Spectroscopic Studies of Fluorenone Derivatives. *J. Fluoresc.* **2001**, *11*, 65−73. (f) Biczók, L.; Bérces, T.; Inoue, H. Effects of Molecular Structure and Hydrogen Bonding on the Radiationless Deactivation of Singlet Excited Fluorenone Derivatives. *J. Phys. Chem. A* **1999**, *103*, 3837−3842. (g) Yatsuhashi, T.; Nakajima, Y.; Shimada, T.; Inoue, H. Photophysical Properties of Intramolecular Charge-Transfer Excited Singlet State of Amino-fluorenone Derivatives. *J. Phys. Chem. A* **1998**, *102*, 3018−3024.

(7) Homnick, P. J.; Lahti, P. M. Modular Electron Donor Group Tuning of Frontier Energy Levels in Diarylaminofluorenone Push−Pull Molecules. *Phys. Chem. Chem. Phys.* **2012**, *14*, 11961−11968.

(8) Rathnayake, H. P.; Cirpan, A.; Karasz, F. E.; Odoi, M. Y.; Hammer, N. I.; Barnes, M. D.; Lahti, P. M. Luminescence of Molecular and Block Copolymeric 2,7-Bis(phenylethenyl)-fluorenones; Identifying Green-band Emitter Sites in a Fluorene-Based Luminophore. *Chem. Mater.* **2007**, *19*, 3265−3270.

(9) For more details about estimating molecular orbital energies from voltammetric potentials, see (a) Pommerehne, J.; Vestweber, H.; Guss, W.; Mahrt, R. F.; Bassler, H.; Porsch, M.; Daub, J. Efficient Two Layer LEDs on a Polymer Blend Basis. *Adv. Mater.* **1995**, *7*, 551−554. (b) Johansson, T.; Mammo, W.; Svensson, M.; Andersson, M.; Inganäs, O. Electrochemical Bandgaps of Substituted Polythiophenes. *J. Mater. Chem.* **2003**, *13*, 1316−1323. (c) Sun, Q.; Wang, H.; Yang, C.; Li, Y. Synthesis and Electroluminescence of Novel Copolymers containing Crown Ether Spacers. *J. Mater. Chem.* **2003**, *13*, 800−806. (d) Cardona, C. M.; Li, W.; Kaifer, A. E.; Stockdale, D.; Bazan, G. C. Electrochemical Considerations for Determining Absolute Frontier Orbital Energy Levels of Conjugated Polymers for Solar Cell Applications. *Adv. Mater.* **2011**, *23*, 2367−2371.

(10) Gaussian 09: Frisch, M. J.; et al. Gaussian 09, revision B.01 ed.; Gaussian, Inc: Wallingford CT, 2010. A full citation is given in the Supporting Information.

(11) (a) Lee, C.; Yang, W.; Parr, R. G. Development of the Colle-Salvetti Correlation-Energy Formula into a Functional of the Electron Density. *Phys. Rev. B* **1988**, *37*, 785−789. (b) Becke, A. D. Density-Functional Thermochemistry. III. The Role of Exact Exchange. *J. Chem. Phys.* **1993**, *98*, 5648/1−5648/5. (c) Stephens, P. J.; Devlin, F. J.; Chabalowski, C. F.; Frisch, M. J. Ab Initio Calculation of Vibrational Absorption and Circular Dichroism Spectra Using Density Functional Force Fields. *J. Phys. Chem.* **1994**, *98*, 11623−11627.

(12) Dennington, R.; Keith, T.; Millam, J. *GaussView*, version 5; Semichem Inc.: Shawnee Mission, KS, 2009.

(13) Aihara, J. Anomalous Solvatochromism of Charge-Transfer Absorption Bands. *Bull. Chem. Soc. Jpn.* **1981**, *54*, 1561−1562 We thank a referee for bringing this reference to our attention.

(14) Solvatochromic red shifts in polar solvents are commonly used as evidence of charge transfer in electronic transitions, as in the following examples: (a) Grabowski, Z. R.; Rotkiewicz, K.; Rettig, W. Structural Changes Accompanying Intramolecular Electron Transfer: Focus on Twisted Intramolecular Charge-Transfer States and Structures. *Chem. Rev.* **2003**, *103*, 3899−4031. (b) Martínez-Martínez, V.; Limb, J.; Bañuelosa, J.; López-Arbeloa, I.; Miljanić, O. Š. Strong Intramolecular Charge Transfer Emission in Benzobisoxazole Cruciforms: Solvatochromic Dyes as Polarity Indicators. *Phys. Chem. Chem. Phys.* **2013**, *15*, 18023−18029. (c) Ooyama, Y.; Oda, Y.; Mizumo, T.; Ohshita, J. Specific Solvatochromism of D-π-A type Pyridinium Dyes Bearing Various Counter Anions in Halogenated Solvents. *Tetrahedron* **2013**, *69*, 1755−1760. (f) Vasilev, A. A.; De Mey, K.; Asselberghs, I.; Clays, K.; Champagne, B.; Angelova, S. E.; Spassova; Chen Li, M. I.; Müllen, K. Enhanced Intramolecular Charge Transfer in New Type Donor−Acceptor Substituted Perylenes. *J. Phys. Chem. C* **2012**, *116*, 22711−22719. (g) Hu, R.; Lager, E.; Aguilar-Aguilar, A.; Liu, J.; Lam, J. W. Y.; Sung, H. H. Y.; Williams, I. D.; Zhong, Y.; Wong, S. S.; Pena-Cabrera, E.; Tang, B. Z. Twisted Intramolecular Charge Transfer and Aggregation-Induced Emission of BODIPY Derivatives. *J. Phys. Chem. C* **2009**, *113*, 15845−15853. (h) Jenekhe, S. A.; Lu, L.; Alam, M. M. New Conjugated Polymers with Donor-Acceptor Architectures: Synthesis and Photophysics of Carbazole-Quinoline and Phenothiazine-Quinoline Copolymers and Oligomers Exhibiting Large Intramolecular Charge Transfer. *Macromolecules* **2001**, *34*, 7315−7324.

(15) Heckmann, A.; Lambert, C. Organic Mixed-Valence Compounds: A Playground for Electrons and Holes. *Angew. Chem., Int. Ed.* **2012**, *51*, 326−392.

(16) Estrada, L. A.; Neckers, D. C Synthesis and Photophysics of Ambipolar Fluoren-9-ylidene Malononitrile Derivatives. *J. Org. Chem.* **2009**, *74*, 8484−8487.

(17) Scalmani, G.; Frisch, M. J.; Mennucci, B.; Tomasi, J.; Cammi, R.; Barone, V. Geometries and Properties of Excited States in the Gas Phase and in Solution: Theory and Application of a Time-Dependent Density Functional Theory Polarizable Continuum Model. *J. Chem. Phys.* **2006**, *124*, 094107/1−15 and references therein.

(18) See, for example: (a) Lambert, C.; Nöll, G. The Class II/III Transition in Triarylamine Redox Systems. *J. Am. Chem. Soc.* **1999**, *121*, 8434-8442, and more generally, (b) Richard, D. E.; Taube, H. Mixed-Valence Molecules: Electronic Delocalization and Stabilization. *Coord. Chem. Rev.* **1984**, *60*, 107−129.

(19) See, for example: (a) Lincker, F.; Attias, A.-J.; Mathevet, F.; Heinrich, B.; Donnio, B.; Fave, J.-L.; Rannou, P.; Demadrille, R. Influence of Polymorphism on Charge Transport Properties in

Isomers of Fluorenone-Based Liquid Crystalline Semiconductors. *Chem. Commun.* **2012**, *48*, 3209−3211. (b) Porzio, W.; Destri, S.; Pasini, M.; Giovanella, U.; Ragazzi, M.; Scavia, G.; Kotowski, D.; Zottib, G.; Vercelli, B. Synthesis and Characterization of Fluorenone-Thiophene-Based Donor-Acceptor Oligomers: Role of Moiety Sequence upon Packing and Electronic Properties. *New J. Chem.* **2010**, *34*, 1961−1973. (b) Vijayakumar, C.; Saeki, A.; Seki, S. Optoelectronic Properties of Dicyanofluorene-Based n-Type Polymers. *Chem.—Asian J.* **2012**, *7*, 1845−1852. (c) Usta, H.; Risko, C.; Wang, Z.; Huang, H.; Deliomeroglu, M. K.; Zhukhovitskiy, A.; Facchetti, A.; Marks, T. J. Design, Synthesis, and Characterization of Ladder-Type Molecules and Polymers. Air-Stable, Solution-Processable *n*-Channel and Ambipolar Semiconductors for Thin-Film Transistors via Experiment and Theory. *J. Am. Chem. Soc.* **2009**, *131*, 5586−5608.

(20) Wong, W.-Y.; Lu, G.-L.; Choi, K.-H.; Lin, Z. Functionalization of 9-(Dicyanomethylene)fluorene Derivatives with Substituted Acetylenes. *Eur. J. Org. Chem.* **2003**, 365−373.

(21) See, for example: (a) Graham, K. R.; Stalder, R.; Wieruszewski, P. M.; Patel, D. G.; Salazar, D. H.; Reynolds, J. R. Tailor-Made Additives for Morphology Control in Molecular Bulk-Heterojunction Photovoltaics. *ACS Appl. Mater. Interfaces* **2013**, *5*, 63−71. (b) Subbiah, J.; Amb, C. M.; Reynolds, J. R.; So, F. Effect of Vertical Morphology on the Performance of Silole-containing Low-Bandgap Inverted Polymer Solar Cells. *Sol. Energy Mater. Sol. Cells* **2012**, *97*, 97−101. (a) Li, R.; Hu, W.; Liu, Y.; Zhu, D. Micro- and Nanocrystals of Organic Semiconductors. *Acc. Chem. Res.* **2010**, *43*, 529−440. (b) Anthony, J. E. *Angew. Chem., Int. Ed.* **2008**, *47*, 452−483. (c) Würthner, F.; Schmidt, R. Electronic and Crystal Engineering of Acenes for Solution-processible Self-assembling Organic Semiconductors. *Chem. Phys. Chem.* **2006**, *7*, 793−797.